NANO LETTERS

Letter

pubs.acs.org/NanoLett

# Graphene-Based Microbots for Toxic Heavy Metal Removal and Recovery from Water

Diana Vilela,[†] Jemish Parmar,[†,‡] Yongfei Zeng,[§] Yanli Zhao,[§] and Samuel Sánchez*[,†,‡,∥]

[†]Max-Planck Institute for Intelligent Systems, Heisenbergstr. 3, 70569 Stuttgart, Germany

[‡]Institute for Bioengineering of Catalonia (IBEC), Baldiri I Reixac 10-12, 08028 Barcelona, Spain

[§]Division of Chemistry and Biological Chemistry, School of Physical and Mathematical Sciences, Nanyang Technological University, 21 Nanyang Link, 637371 Singapore, Singapore

[∥]Institució Catalana de Recerca i Estudis Avançats (ICREA), Psg. Lluís Companys, 23, 08010 Barcelona, Spain

*S* *Supporting Information*

**ABSTRACT:** Heavy metal contamination in water is a serious risk to the public health and other life forms on earth. Current research in nanotechnology is developing new nanosystems and nanomaterials for the fast and efficient removal of pollutants and heavy metals from water. Here, we report graphene oxide-based microbots (GOx-microbots) as active self-propelled systems for the capture, transfer, and removal of a heavy metal (i.e., lead) and its subsequent recovery for recycling purposes. Microbots' structure consists of nanosized multilayers of graphene oxide, nickel, and platinum, providing different functionalities. The outer layer of graphene oxide captures lead on the surface, and the inner layer of platinum functions as the engine decomposing hydrogen peroxide fuel for self-propulsion, while the middle layer of nickel enables external magnetic control of the microbots. Mobile GOx-microbots remove lead 10 times more efficiently than nonmotile GOx-microbots, cleaning water from 1000 ppb down to below 50 ppb in 60 min. Furthermore, after chemical detachment of lead from the surface of GOx-microbots, the microbots can be reused. Finally, we demonstrate the magnetic control of the GOx-microbots inside a microfluidic system as a proof-of-concept for automatic microbots-based system to remove and recover heavy metals.

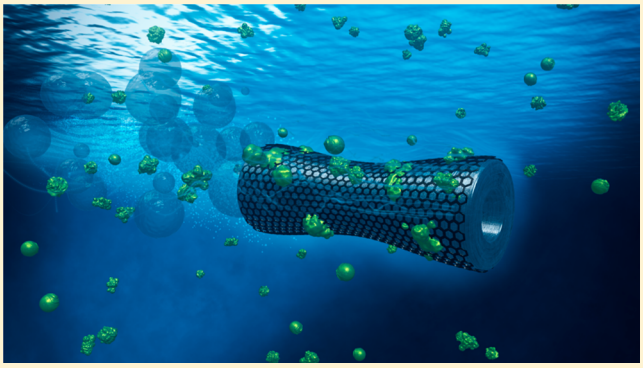

**KEYWORDS:** *Graphene, heavy metals, microbots, catalytic microswimmers, wastewater treatment, metal recovery, environmental application*

Pollution in water from heavy metals such as arsenic, mercury, cadmium, chromium, and lead, originates from various human industrial activities such as electroplating, mining, fabrication of batteries and microelectronics. It is a potential hazard to living systems; hence, it is essential to develop efficient and inexpensive materials and technologies to remove and recycle them from polluted water. Various methods are in use to remove and recover heavy metals such as chemical precipitation, adsorption, ion exchange, and membrane filtration among which adsorption is considered an economical and effective strategy.[1]

Recent developments in nanotechnology have further increased the effectiveness of adsorbent materials providing innovative systems for improving environmental remediation.[2,3] Lately, numerous reports described the utilization of graphene and its composites as good adsorbents for the removal of dyes and heavy metal ions from aqueous solutions.[4−6] Furthermore, in the last couple of years, catalytic self-propelled micro- and nanomotors have demonstrated diverse applications within the environmental field. The synergy between active motion of micromotors,[7−10] which enhances micromixing (and mass transfer in the solution[11,12] and surface multifunctionalities[13,14] opens many possibilities of artificial swimmers as water remediation tools.[11,15,16] For instance, they are very efficient in the degradation of organic pollutants,[11,17−20] chemical warfare agents,[21,22] and the capture of organics[23−29] from water. They can analyze the water quality from the fluid where they swim such as the detection of heavy metals,[30,31] pH,[32] or other analytes.[33−35] However, reusable micromotors for the capture and release of heavy metals in defined locations have not been yet reported.

Here, we present the removal and recovery of heavy metals (lead) from contaminated water by using graphene oxide (GOx) based tubular micromotors, dubbed microbots, propelled by a catalytic reaction. The high adsorption of Pb (II) ions on the graphene oxide (GOx) nanosheets of the microbots surface is a spontaneous process due to the strong surface complexation

**Received:** February 22, 2016
**Revised:** March 15, 2016
**Published:** March 21, 2016

  

DOI: 10.1021/acs.nanolett.6b00768
*Nano Lett.* 2016, 16, 2860−2866

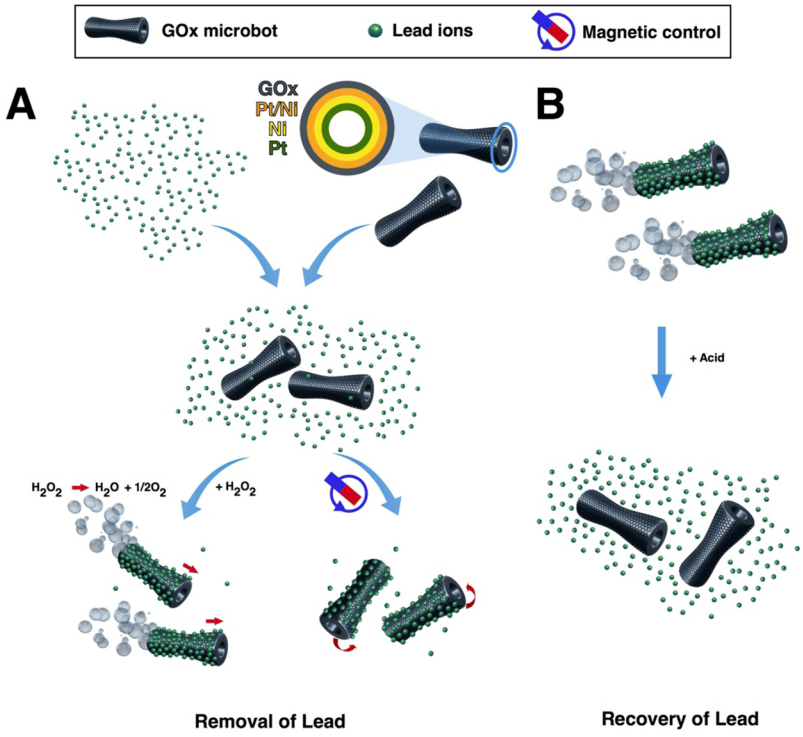


**Figure 1.** Scheme of GOx-microbots based approach for lead decontamination and recovery. (A) Decontamination of polluted water using GOx-microbots fabricated by electrodeposition of nanolayers of graphene oxide (GOx), Pt/Ni layer, Ni magnetic layer, and Pt catalytic inner layer. The decontamination strategy for lead ions can be carried out by two different techniques: self-propulsion of the GOx-microbots in the presence of $H_2O_2$ or by using an external rotating magnetic field. (B) Recovery of lead ions from the GOx-microbots in the presence of acidic media.

between the Pb (II) ions and the abundant oxygen moieties on the GOx. Moreover, due to the magnetic properties of these microbots, they can be easily removed from the water using a magnet after successful lead decontamination. The adsorbed Pb(II) ions on the microbots can be recovered via acid pH adjustment allowing them to be recycled and reused for further decontamination processes.

The detailed fabrication of conical, self-propelled tubular motors by sequential electrochemical deposition of nanolayers on the inner wall of a polycarbonate membrane is described in the Supporting Information (SI). As shown in Figure 1A, the microbot structure consists of an outer graphene layer and a platinum inner layer. The platinum layer decomposes hydrogen peroxide into water and oxygen microbubbles, and the ejection of microbubbles from one side of microbot provides enough force for its self-propulsion. Between the Pt and GOx, layers of Pt/Ni and Ni were deposited to control and guide microbots motion by externally applied magnetic field.

Taking advantage of the self-propulsion and magnetic characteristics of the microbots, in combination with the GOx adsorption properties to attach Pb (II) ions, two approaches for the water cleaning of lead were carried out (Figure 1A). In addition, the recovery of lead after its removal from wastewater is also carried out, as it is displayed in Figure 1B.

GOx-microbots were characterized by scanning electron microscopy (SEM), energy dispersive X-ray spectroscopy (EDX), Raman spectroscopy, and high resolution X-ray photoelectron spectroscopy (XPS), as it is observed in Figure 2. Figure 2A,1 illustrates the tubular morphology and size polydispersity of the microbots after their fabrication. Most of the microbots show biconical morphology and a low polydispersity indicating that fabrication was homogeneous. Figure 2A,2 displays the hollow inside layer of a representative microbot. Their average outer diameter is $4.6 \pm 0.1$ $\mu$m ($n = 10$) and their inner diameter $2.5 \pm 0.1$ $\mu$m ($n = 10$). The surface of microbots is not homogeneous, as it is shown in Figure 2A,3 which can be due to the high number of defects produced by the electrochemical deposition of graphene nanosheets on the polycarbonate membrane during the fabrication of these microbots. Figure 2B illustrates the EDX analysis and reveals the components of the microbots including carbon, nickel, and platinum where platinum is the major component. Raman spectroscopy analysis and mapping for GOx-microbots are shown in Figure 2C and D, respectively. Figure 2C shows Raman spectrum of the microbot surface where the characteristic peaks of D and G band are observed at 1350 and 1570 $cm^{-1}$, respectively. Usually, the D-mode is caused by disordered structure of graphene, while band G arises from the stretching of the C−C bond in graphitic materials and is common to all $sp^2$ carbon systems. The band intensity ratio of $I_D/I_G$ suggests the presence of oxidated carbon in GOx-microbots. To further confirm the complete coverage of GO layer on microbots, the GOx-microbots were characterized by confocal Raman technique. As shown in the bright field image (Figure 2D inset), a trimer of GOx-microbots formed by physical attachment was chosen for the Raman mapping. By mapping integrated intensity values of D and G bands in Raman spectrum of GOx-microbots, a 2-D Raman line mapping image was acquired and is presented in Figure 2D. A homogeneous distribution of high intensity signal in red and yellow colors resembles the width of the trimmer with similar dimensions. The confocal Raman line mapping image confirmed the successful and uniform coverage of GO on the surface of microbots. XPS spectra survey further reveals the presence of carbon (C 1s peak) and oxygen (O 1s peak) elements on the surface of GOx-


DOI: 10.1021/acs.nanolett.6b00768
Nano Lett. 2016, 16, 2860−2866

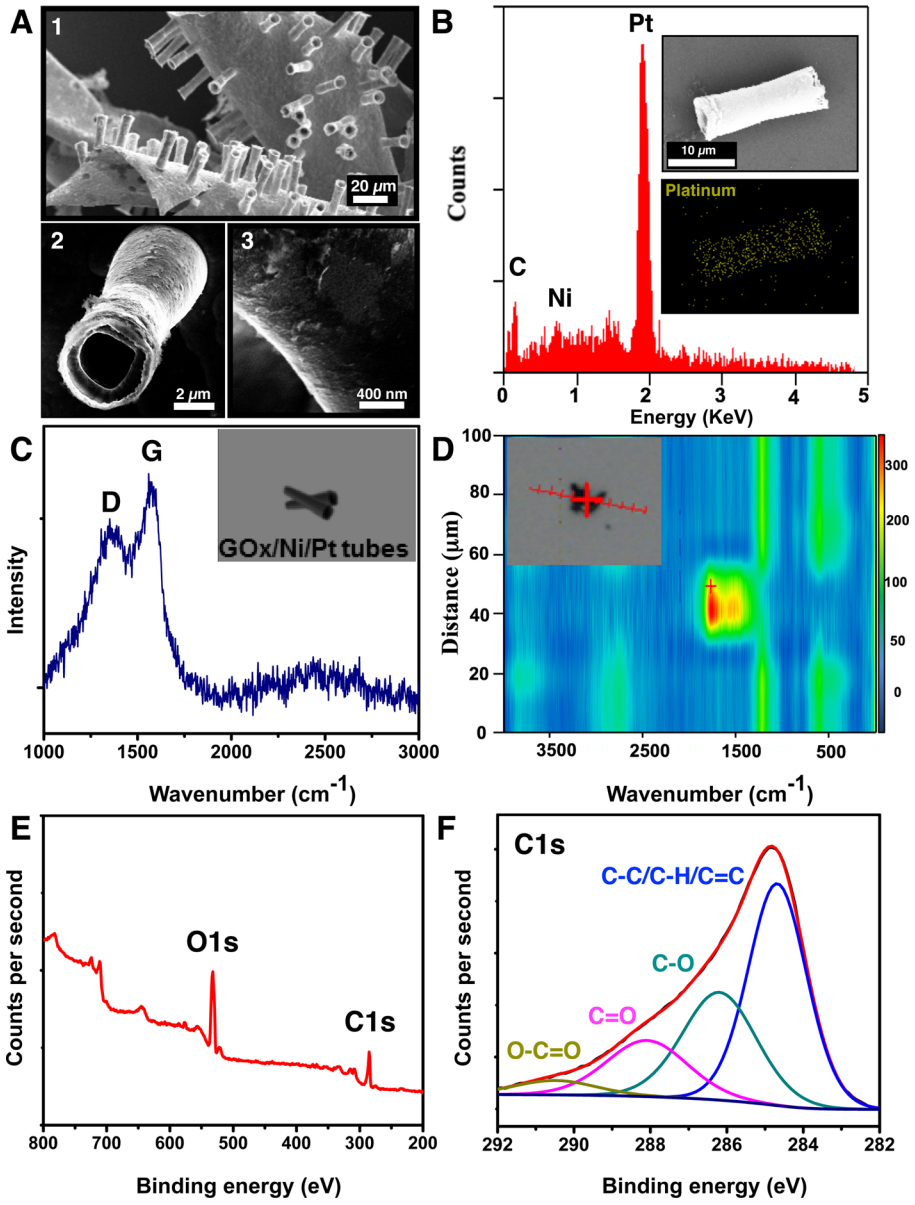


**Figure 2.** Characterization of GOx-microbots: (A) SEM images illustrating: (1) GOx-microbots attached to the gold layer, (2) structure of a single GOx-microbot, and (3) close look of the surface of a GOx-microbot. (B) The EDX spectrum of GOx-microbots (inset: EDX mapping of the GOx-microbot for Pt). (C) Raman spectrum from the surface of GOx-microbots, showing characteristic D and G band of graphene oxide. (Inset is an illustration of the GOx-microbots analyzed by Raman spectroscopy.) (D) Raman spectroscopy displays the Raman scan map of the GOx-microbots, confirming the presence of graphene on the full surface of microbots (see inset: image of the GOx/Ni/Pt tube and scanning path (red line) of the analysis). (E) XPS spectra survey of GOx-microbots, showing O 1s and C 1s peaks. (F) High-resolution C 1s XPS spectra of GOx microbots displaying various functional groups identified on the surface.

microbots, where the O 1s signal is higher compared to the C 1s signal (Figure 2E) characteristic for GOx. The peaks of high-resolution C 1s spectra (Figure 2F) and O 1s spectra (Figure S1) correspond to the binding energy of various functional groups such as C−C/C−H/C═C, C−OH, C═O, and O−C═O, revealing the nature of the covalent bonds of oxygen atoms and carbon atoms (Table S1). The ratio of percentage atomic concentration of C−C/C−H/C═C functional groups to all carbon−oxygen functional groups is 0.94, which denotes the degree oxidation of GOx. Abundant carbonyl and carboxyl groups are present on the GOx-microbots which are considered very important for the adsorption of heavy metals on the surface of graphene oxide.[36]

To prove the capability of the self-propelled GOx-microbots for the purification of lead contaminated water by adsorption, a concentration of 1.5% (v/v) of $H_2O_2$ and 0.1% (w/v) of sodium dodecyl sulfate (SDS) were used systematically in the all experiments as the optimal conditions for the swimming of the GOx-microbots. Average velocities of the microbots in these conditions were around 500 $\mu m\ s^{-1}$. A swarm of approximately $2 \times 10^5$ GOx-microbots was deployed in the lead contaminated water (1 ppm) for adsorptive removal. Figure 3A shows snapshots from characteristic microbots swimming in lead-contaminated water at different time periods. Bubble tails released from microbots indicate the trajectories and displacement of microbots at initial time, 15, 30, and 60 min, respectively.



DOI: 10.1021/acs.nanolett.6b00768
Nano Lett. 2016, 16, 2860−2866

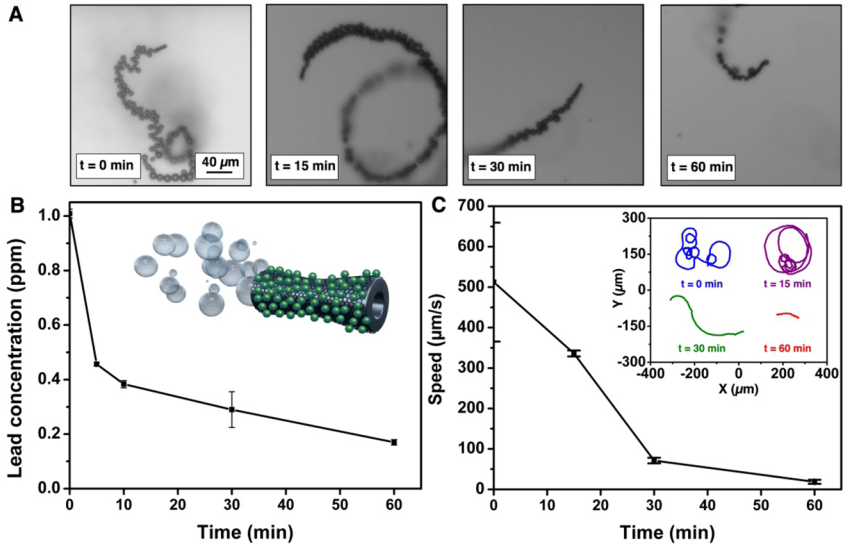


**Figure 3.** Kinetics of Pb(II) decontamination and speed for the GOx-microbots. (A) Optical snapshots from videos of GOx-microbots moving at different times during the decontamination process. (B) Pb(II) ion concentration at different time intervals during decontamination by GOx-microbots (inset: illustration of a GOx-microbot with adsorbed lead (green dots) on the surface after the decontamination process). (C) Speed of GOx-microbots at different times (0, 15, 30, and 60 min, inset: trajectories of the GOx-microbots for 5 s). Experimental conditions: 1 ppm as initial Pb(II) concentration, 1.5% (v/v) of $H_2O_2$ and 0.1% (w/v) SDS.

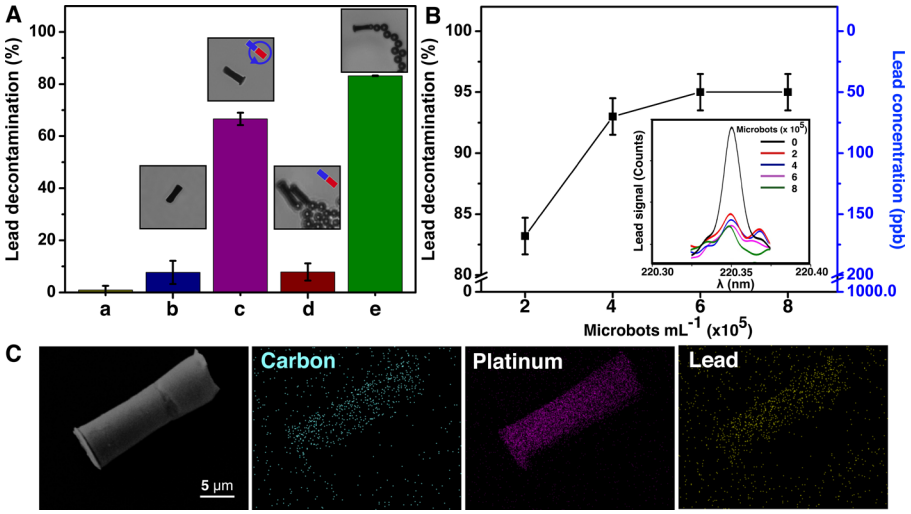


**Figure 4.** Pb (II) ions decontamination by GOx-microbots and characterization of microbots after decontamination. (A) Decontamination of Pb(II) ions in different systems: In the presence of (a) $H_2O_2$ (1.5% v/v) and of SDS (0.1% w/v) after 24 h, (b) SDS (0.1% w/v) and nonmotile GOx- microbots after 1 h, (c) SDS (0.1% w/v) and GOx-microbots stirred by external magnets after 1 h, (d) $H_2O_2$ (1.5% v/v), SDS (0.1% w/v) and docked GOx-microbots after 1 h (immobilized by stationary magnetic field), and (e) in the presence of $H_2O_2$ (1.5% v/v) and SDS (0.1% w/v) motile GOx-microbots after 1 h. (B) Decontamination of Pb(II) ions for different concentrations of GOx-microbots after 1 h in the presence of $H_2O_2$ (1.5% v/v) and of SDS (0.1% w/v). (Inset: ICP-OES signal of lead concentration after 1 h of decontamination process for increasing amount of motors.) (C) EDX mapping: the SEM image of the analyzed GOx-microbot after the decontamination process showing, carbon distribution, platinum distribution, and Pb(II) distribution.

Figure 3B shows the decrease in lead concentration over 60 min in the presence of motile GOx-microbots. The lead concentration was measured using inductively coupled plasma optical emission spectrometry (ICP-OES) which is able to detect traces of metals. In the first 10 min, the GOx-microbots were able to decrease the lead concentration from 1 ppm to lower than 0.4 ppm, and in 1 h the GOx-microbots were able to remove more than the 80% of lead from the contaminated water. The GOx-microbots were allowed to swim for 24 h observing that after this time the concentration of lead was slightly higher (0.29 ± 0.02 ppm) than it was in 1 h (0.17 ± 0.01 ppm). This could be attributed to the fact that with time, the process of adsorption reaches to a desorption−adsorption equilibrium where desorption phenomenon could also occur. Therefore, 1 h was selected as the optimal time for the lead remediation from polluted water. Figure 3C (inset) and Video 1 (SI) displays the tracking of the average speed of the microbots for 5 s at different times (0, 15, 30, and 60 min). When the microbots were initially added to the lead contaminated solution and 1.5% $H_2O_2$ (v/v), high velocities and frequent reorientation of trajectories were observed. After 15 min, the speed of the microbots slightly decreased, and their trajectories were usually circular or straight. After 30 and 60 min,



DOI: 10.1021/acs.nanolett.6b00768
Nano Lett. 2016, 16, 2860−2866

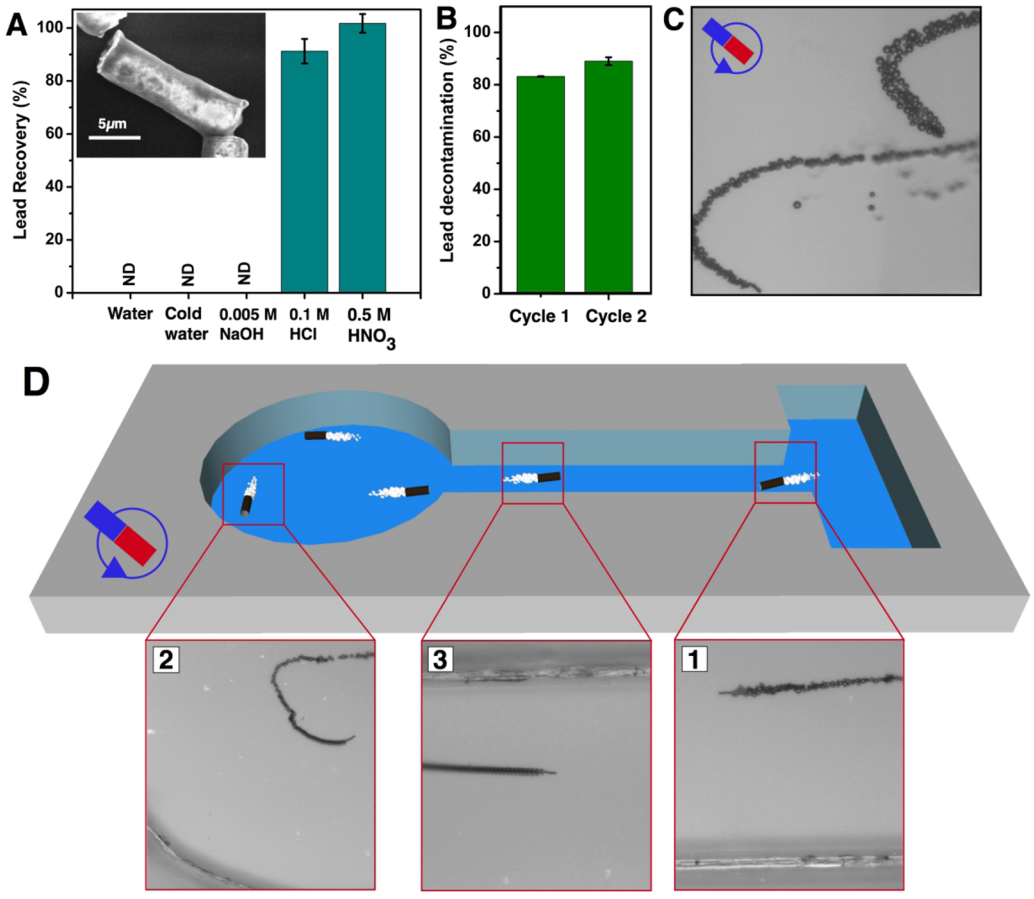


**Figure 5.** Lead recovery, reusability and magnetic control of GOx-micromotors. (A) Recovery of Pb(II) ions from GOx-microbots after different desorption treatments for 1 h, which were previously employed in decontamination process. (Inset shows SEM image illustrating GOx-microbot tube after the decontamination and desorption (with 0.5 M $HNO_3$) process. (B) Reusability of GOx-microbots, representing lead decontamination in the first and second cycle. (C) Optical snapshot from a video of GOx-microbot controlled by magnetic guidance after the lead recovery process. (D) GOx-microbot controlled by magnetic guidance swimming in a PDMS microchannel as a prototype system. Experimental conditions for B and C: 1.5% (v/v) of $H_2O_2$ and 0.1% (w/v) of SDS.

microbots swam at slower speed compared to their initial values and with less frequent reorientation in the direction of swimming. This swimming behavior was due to the fact that the $H_2O_2$ was being consumed continuously from the solution during the catalytic reaction on the inner platinum surface. To demonstrate that the presence of lead does not affect the motor speeds, new $H_2O_2$ was added to the slow or nonswimming microbots that had previously undergone 24 h of catalytic reaction. Addition of the fresh $H_2O_2$ reestablished microbot swimming with similar velocities and movements as were observed at the beginning of the experiments.

Control experiments were carried out to demonstrate that the decontamination process was due to the adsorption on the GOx-microbots (Figure 4). Figure 4A,a shows that without the use of microbots, the lead concentration does not decrease when in contact with the fuel $H_2O_2$ and SDS after 24 h. Figure 4A,b shows minor decontamination of lead when a fixed amount of GOx-microbots were left in contact with the lead contaminated solution for 1 h. This was performed without adding $H_2O_2$ in the solution, so that GOx-microbots could not swim, leading to a low decontamination of lead. The GOx-microbots were then stirred by rotation of an external magnetic field generated by the magnetic stirrer, as it is represented in the inset in Figure 4A,c. Here, microbots were able to remove 66.6 ± 2.4% lead from water. When the GOx-microbots are rotated at high speed in the solution, the diffusion of lead ions on the microbot surface is enhanced due to induced microconvection. This increases the chances of contact between contaminant and microbots. Figure 4A,d displays the decontamination when the bubbled GOx-microbots left in polluted solution, but their swimming was inhibited by the presence of a strong magnet, which immobilizes them in a fixed location. However, when these GOx-microbots were left free to swim (Figure 4A,e), the decontamination process is 10 times more effective as it varies from 7.7 ± 4.5% (nonmotile) to 83.2 ± 1.0% (motile). These results reveal the high significance of the synergy between the presence of graphene oxide and self-propulsion of the GOx-microbots.

Because the lead decontamination is an adsorption process based on the adhesion of lead onto a GOx surface, when the number of GOx-microbots in the contaminated water was increased, the concentration of lead in the solution decreased as displayed in Figure 4B. We doubled the number of microbots and up to four times the standardized amount of microbots ($2 \times 10^5$ microbots), resulting in an increase of lead capture from 83.2% to more than 95% (remaining lead concentration was <50 ppb). The plateau at $6 \times 10^5$ microbots indicates the lead detection limit of the analytical system used for the analysis.

EDX mapping was used to verify the decontamination by GOx-microbots, which showed the presence of Pb on their surfaces (Figure 4C). Lead was not found in EDX mapping



DOI: 10.1021/acs.nanolett.6b00768
*Nano Lett.* 2016, 16, 2860−2866

performed previous to the decontaminating experiment (Figure 1B), which gives direct evidence of adsorption of lead on the surface of the microbots. The effective adsorption of lead on graphene surface of the GOx-microbots is based on the strong interactions produced between graphene oxide and Pb (II) ions due to the formation of electron donor−acceptor complexes. The presence of oxygen moieties and delocalized $\pi$-electron systems in graphene oxide act as Lewis base and attach to the Pb(II) ions which act as Lewis acid. In addition, this process is strongly dependent on the pH and temperature and independent of ionic strength.[37] We also observed that the structure of the GOx-microbots was not damaged by the decontamination process maintaining its composition (Figure 4C, SEM image).

We further demonstrate the recovery of lead after its removal from polluted water. Figure 5A shows the efficiency of lead recovery after treating GOx-microbots in different chemical conditions to induce the desorption of Pb(II) from their surfaces (see SI). Different aliquots of previously used GOx-microbots for lead removal were extracted using a magnet, dissolved in 3 mL of different media (Figure 5A), and stirred for 1 h. After the removal of GOx-microbots from the solution by magnetic control, the remaining solution was analyzed for lead by ICP-OES analysis. When the GOx-microbots were in the presence of water, cold water (temp 4 °C), and basic pH (11), the Pb(II) ion concentration was not detectable at the detection limit of the instrument (50 ppb). However, when the GOx-microbots were in the presence of acidic media, i.e., HCl (pH = 1) and $HNO_3$ (pH = 0.3), a desorption event reached recoveries up to 91.2 ± 4.6% and 101.0 ± 3.5%, respectively. The structure of the GOx-microbots was not significantly affected as it is observed in the inset of Figure 5A which shows a SEM image of GOx-microbot after the decontamination and recovery processes. After cleaning and washing GOx-microbots, the reusability of GOx-microbots was studied. The GOx-microbots were added into the lead contaminated water as the first decontamination assays. Figure 5B represents that the GOx microbots retained their lead removal efficiently in the second cycle after removing and recovering lead in the first cycle. Activation of graphene oxide by treatment with the oxidant acids such as nitric acids oxidize the graphene surface and increase the number of oxygen moieties, which mainly interact with Pb(II) ions.

As a proof-of-concept, we tested the capabilities of GOx-microbots to perform various tasks inside a PDMS microchannel by external magnetic guidance. Because GOx-microbots contain Ni layer, they are ferromagnetic in nature which allows controlling trajectories by external magnetic field once they are self-propelled in solution. Figure 5C and Video 2 (SI) show the trajectory control of GOx-microbots by using the external magnetic field after the process of Pb(II) decontamination on the surface. Figure 5D and Video 3 (SI) illustrate a GOx-microbot guided in the microfluidic channel from the lead contaminated water containing reservoir after decontamination to the other location where lead can be recovered and concentrated for recycling. The ability to magnetically control the microbots makes it possible to develop and program an automated system to guide swarm of microbots to accomplish the assigned tasks.

In conclusion, we have demonstrated graphene oxide based microbots for very efficient removal of toxic heavy metal (Pb) from contaminated water through an adsorption process, the recovery of Pb(II) ions, and the subsequent reusability of GOx-microbots. GOx-microbots can be deployed in contaminated water to swim randomly and easily collected using magnets once the water purification process has been completed. As a proof of the concept, magnetic control of GOx-microbots swimming inside a microfluidic system was demonstrated. GOx-microbots can be useful as new devices for future decontamination of heavy metals from industrial wastewater due to their efficiency for decontamination, their easy removal from the solution and the possibility of lead recovery and their reusability. The use of active systems and graphene nanomaterials can pave the way for new functionalities of self-propelled micronanomotors, from drug delivery, sensing, and energy to new environmental applications.

## ■ ASSOCIATED CONTENT

### Supporting Information

The Supporting Information is available free of charge on the ACS Publications website at DOI: 10.1021/acs.nanolett.6b00768.

Methods (PDF)
Video S1 (AVI)
Video S2 (AVI)
Video S3 (AVI)

## ■ AUTHOR INFORMATION


### Corresponding Author

*E-mail: ssanchez@ibecbarcelona.eu, sanchez@is.mpg.de.

### Present Address

Y.Z.: Key Laboratory of Inorganic−Organic Hybrid Functional Material Chemistry (Ministry of Education), Tianjin Key Laboratory of Structure and Performance for Functional Molecules, College of Chemistry, Tianjin Normal University, Tianjin 300387, P. R China.


### Author Contributions

D.V. and J.P. contributed equally to this work.

### Notes

The authors declare no competing financial interest.

## ■ ACKNOWLEDGMENTS


The results leading to the publication have received financial support from the European Research Council for the European Union's Seventh Framework Programme (FP7/2007-2013)/ERC Grant Agreement 311529 (Lab-in-a-tube and Nanorobotics biosensors) and the Alexander von Humboldt Foundation (DV). Authors thank L. Soler for help with XPS analysis.


## ■ REFERENCES


(1) Fu, F.; Wang, Q. *J. Environ. Manage.* **2011**, *92*, 407−418.
(2) Shannon, M. A.; Bohn, P. W.; Elimelech, M.; Georgiadis, J. G.; Marinas, B. J.; Mayes, A. M. *Nature* **2008**, *452* (7185), 301−310.
(3) Ali, I. *Chem. Rev.* **2012**, *112* (10), 5073−5091.
(4) Zhao, G.; Li, J.; Ren, X.; Chen, C.; Wang, X. *Environ. Sci. Technol.* **2011**, *45* (24), 10454−10462.
(5) Cong, H.-P.; Ren, X.-C.; Wang, P.; Yu, S.-H. *ACS Nano* **2012**, *6* (3), 2693−2703.
(6) Huang, Z.-H.; Zheng, X.; Lv, W.; Wang, M.; Yang, Q.-H.; Kang, F. *Langmuir* **2011**, *27* (12), 7558−7562.
(7) Wang, W.; Duan, W.; Ahmed, S.; Sen, A.; Mallouk, T. E. *Acc. Chem. Res.* **2015**, *48* (7), 1938−1946.
(8) Sánchez, S.; Soler, L.; Katuri, J. *Angew. Chem., Int. Ed.* **2015**, *54* (5), 1414−1444.
(9) Paxton, W. F.; Kistler, K. C.; Olmeda, C. C.; Sen, A.; St. Angelo, S. K.; Cao, Y.; Mallouk, T. E.; Lammert, P. E.; Crespi, V. H. *J. Am. Chem. Soc.* **2004**, *126* (41), 13424−13431.
(10) Wang, H.; Pumera, M. *Chem. Rev.* **2015**, *115* (16), 8704−8735.
(11) Soler, L.; Magdanz, V.; Fomin, V. M.; Sanchez, S.; Schmidt, O. G. *ACS Nano* **2013**, *7* (11), 9611−9620.




DOI: 10.1021/acs.nanolett.6b00768
*Nano Lett.* 2016, 16, 2860−2866

(12) Orozco, J.; Jurado-Sánchez, B.; Wagner, G.; Gao, W.; Vazquez-Duhalt, R.; Sattayasamitsathit, S.; Galarnyk, M.; Cortés, A.; Saintillan, D.; Wang, J. *Langmuir* **2014**, *30* (18), 5082−5087.
(13) Guix, M.; Mayorga-Martinez, C. C.; Merkoçi, A. *Chem. Rev.* **2014**, *114* (12), 6285−6322.
(14) Wang, J. *Nanomachines: fundamentals and applications*; John Wiley & Sons, 2013.
(15) Soler, L.; Sánchez, S. *Nanoscale* **2014**, *6* (13), 7175−7182.
(16) Gao, W.; Wang, J. *ACS Nano* **2014**, *8* (4), 3170−3180.
(17) Li, T.; Li, L.; Song, W.; Wang, L.; Shao, G.; Zhang, G. *ECS J. Solid State Sci. Technol.* **2015**, *4* (10), S3016−S3019.
(18) Wani, O. M.; Safdar, M.; Kinnunen, N.; Jänis, J. *Chem. - Eur. J.* **2016**, *22* (4), 1244−1247.
(19) Mushtaq, F.; Guerrero, M.; Sakar, M. S.; Hoop, M.; Lindo, A. M.; Sort, J.; Chen, X.; Nelson, B. J.; Pellicer, E.; Pane, S. *J. Mater. Chem. A* **2015**, *3* (47), 23670−23676.
(20) Teo, W. Z.; Zboril, R.; Medrik, I.; Pumera, M. *Chem. - Eur. J.* **2016**, *22*, 4789.
(21) Orozco, J.; Cheng, G.; Vilela, D.; Sattayasamitsathit, S.; Vazquez-Duhalt, R.; Valdés-Ramírez, G.; Pak, O. S.; Escarpa, A.; Kan, C.; Wang, J. *Angew. Chem., Int. Ed.* **2013**, *52* (50), 13276−13279.
(22) Li, J.; Singh, V. V.; Sattayasamitsathit, S.; Orozco, J.; Kaufmann, K.; Dong, R.; Gao, W.; Jurado-Sanchez, B.; Fedorak, Y.; Wang, J. *ACS Nano* **2014**, *8* (11), 11118−11125.
(23) Guix, M.; Orozco, J.; García, M.; Gao, W.; Sattayasamitsathit, S.; Merkoçi, A.; Escarpa, A.; Wang, J. *ACS Nano* **2012**, *6* (5), 4445−4451.
(24) Seah, T. H.; Zhao, G.; Pumera, M. *ChemPlusChem* **2013**, *78* (5), 395−397.
(25) Gao, W.; Feng, X.; Pei, A.; Gu, Y.; Li, J.; Wang, J. *Nanoscale* **2013**, *5* (11), 4696−4700.
(26) Singh, V. V.; Martin, A.; Kaufmann, K.; D. S. de Oliveira, S.; Wang, J. *Chem. Mater.* **2015**, *27* (23), 8162−8169.
(27) Jurado-Sánchez, B.; Sattayasamitsathit, S.; Gao, W.; Santos, L.; Fedorak, Y.; Singh, V. V.; Orozco, J.; Galarnyk, M.; Wang, J. *Small* **2015**, *11* (4), 499−506.
(28) Orozco, J.; Mercante, L. A.; Pol, R.; Merkoci, A. *J. Mater. Chem. A* **2016**, *4*, 3371.
(29) Mou, F.; Pan, D.; Chen, C.; Gao, Y.; Xu, L.; Guan, J. *Adv. Funct. Mater.* **2015**, *25* (39), 6173−6181.
(30) Orozco, J.; García-Gradilla, V.; D'Agostino, M.; Gao, W.; Cortés, A.; Wang, J. *ACS Nano* **2013**, *7* (1), 818−824.
(31) Moo, J. G. S.; Wang, H.; Zhao, G.; Pumera, M. *Chem. - Eur. J.* **2014**, *20* (15), 4292−4296.
(32) Dey, K. K.; Bhandari, S.; Bandyopadhyay, D.; Basu, S.; Chattopadhyay, A. *Small* **2013**, *9* (11), 1916−1920.
(33) Vilela, D.; Orozco, J.; Cheng, G.; Sattayasamitsathit, S.; Galarnyk, M.; Kan, C.; Wang, J.; Escarpa, A. *Lab Chip* **2014**, *14* (18), 3505−3509.
(34) Esteban-Fernández de Ávila, B.; Lopez-Ramirez, M. A.; Báez, D. F.; Jodra, A.; Singh, V. V.; Kaufmann, K.; Wang, J. *ACS Sens.* **2016**, DOI: 10.1021/acssensors.5b00300.
(35) Moreno-Guzman, M.; Jodra, A.; López, M.-Á.; Escarpa, A. *Anal. Chem.* **2015**, *87* (24), 12380−12386.
(36) Moo, J. G. S.; Khezri, B.; Webster, R. D.; Pumera, M. *ChemPhysChem* **2014**, *15* (14), 2922−2929.
(37) Zhao, G.; Ren, X.; Gao, X.; Tan, X.; Li, J.; Chen, C.; Huang, Y.; Wang, X. *Dalton Trans.* **2011**, *40* (41), 10945−10952.



DOI: 10.1021/acs.nanolett.6b00768
*Nano Lett.* 2016, 16, 2860−2866